

Kondo interaction in FeTe and its potential role in the magnetic order

Younsik Kim^{1,2}, Minsoo Kim^{1,2}, Min-Seok Kim³, Cheng-Maw Cheng⁴, Joonyoung Choi⁵, Saegyeol Jung^{1,2}, Donghui Lu⁶, Jong Hyuk Kim⁷, Soohyun Cho⁸, Dongjoon Song^{1,2}, Dongjin Oh^{1,2}, Li Yu^{9,10,11}, Young Jai Choi⁷, Hyeong-Do Kim¹², Jung Hoon Han¹³, Younjung Jo⁵, Jungpil Seo³, Soonsang Huh^{1,2*}, Changyoung Kim^{1,2*}

¹Center for Correlated Electron Systems, Institute for Basic Science, Seoul 08826, Korea

²Department of Physics & Astronomy, Seoul National University, Seoul 08826, Korea

³Department of Emerging Materials Science, DGIST, Daegu 42988, South Korea

⁴National Synchrotron Radiation Research Center, Hsinchu 300, Taiwan

⁵Department of Physics, Kyungpook National University, Daegu 38869, Korea

⁶Stanford Synchrotron Radiation Light source, SLAC National Accelerator Laboratory, CA 94025, USA

⁷Department of Physics, Yonsei University, Seoul 03021, Korea

⁸Center for Excellence in Superconducting Electronics, State Key Laboratory of Functional Materials for Informatics, Shanghai Institute of Microsystem and Information Technology, Chinese Academy of Sciences, Shanghai 200050, China

⁹Beijing National Laboratory for Condensed Matter Physics and Institute of Physics, Chinese Academy of Sciences, Beijing 100190, China

¹⁰School of Physical Sciences, University of Chinese Academy of Sciences, Beijing 100049, China

¹¹Songshan Lake Materials Laboratory, Dongguan, Guangdong 523808, China

¹²XFEL Beamline Division, Pohang Accelerator Laboratory, Pohang 37673, Korea

¹³Department of Physics, Sungkyunkwan University, Suwon 16419, Korea

*Corresponding author. Email: sshuhss@gmail.com (S. H.); changyoung@snu.ac.kr (C. K.)

ABSTRACT

Finding *d*-electron heavy fermion (HF) states has been an important topic as the diversity in *d*-electron materials can lead to many exotic Kondo effect-related phenomena or new states of matter such as correlation-driven topological Kondo insulator or cooperation between long-range magnetism and Kondo lattice behavior. Yet, obtaining direct spectroscopic evidence for a *d*-electron HF system has been elusive to date. Here, we report the observation of Kondo lattice behavior in an antiferromagnetic metal, FeTe, via angle-resolved photoemission spectroscopy (ARPES) and transport properties measurements. The Kondo lattice behavior is represented by the emergence of a sharp quasiparticle at low temperatures. The transport property measurements confirm the low-temperature Fermi liquid behavior and reveal successive coherent-incoherent crossover upon increasing temperature. We interpret the Kondo lattice behavior as a result of hybridization between localized Fe $3d_{xy}$ and itinerant Te $5p_z$ orbitals. Our interpretation is further evidenced by Fano-type tunneling spectra which accompany a hybridization gap. Our observations strongly suggest unusual cooperation between Kondo lattice behavior and long-range magnetic order.

I. INTRODUCTION

Coupling between spin and electronic degrees of freedom in condensed matter systems leads to a variety of emergent phenomena such as colossal magnetoresistance, Rashba effect, anomalous Hall effect, and unconventional superconductivity [1-5]. In particular, understanding how the spin and electronic degrees of freedom interact in such systems is the key to elucidating the underlying physical mechanism and can thus be a steppingstone to future practical applications.

One of the canonical fields to study the interplay of these degrees of freedom is heavy fermion materials [6, 7]. Heavy fermion states appear as a result of the interaction between itinerant electrons and localized magnetic moments, known as Kondo interaction. Previous experimental/theoretical studies show most of the heavy fermion materials are f-electron systems [3, 6, 7]. It was only recently proposed that d-electron systems can also host HF states via Kondo interactions [8-11]. HF states in d-electron materials are especially important due to the possibility that the diversity of d-electron systems may result in exotic Kondo interaction-related phenomena, such as topological Kondo insulating state [12] or cooperation between Kondo lattice behavior and long-range magnetism [13]. Thus, the novelty calls for new studies to find HF in d-electron material groups.

FeTe can be a candidate material to observe d-electron HF states. Its electron correlation is the strongest among the iron-based superconductors (IBSCs) [14]. The magnetic ground state is known to be bicollinear antiferromagnetism (BAFM) with a large magnetic moment of $2.1 \mu_B$, implying its local nature of the magnetism [14]. The Sommerfeld coefficient of FeTe is reported to be $31.4 \text{ mJ}/(\text{K}^2 \cdot \text{mol})$, indicating a heavy effective mass of the system [15]. This value is much larger than that of other iron chalcogenides; FeS and FeSe for instance have 3.8 and $6.9 \text{ mJ}/(\text{K}^2 \cdot \text{mol})$, respectively [16, 17].

In addition to these HF-related properties, other transport properties suggest the existence of strong spin-electron interaction. The temperature-dependent resistivity exhibits a drastic change at the Néel temperature (T_N). It shows an insulating behavior above T_N , but a metallic behavior below T_N [18]. The aforementioned properties of FeTe imply that the local magnetic moment significantly affects the electronic structure. Thus, electronic structure studies on the HF state of FeTe can unveil its origin and how it couples with magnetism.

Here, we report on a comprehensive study on FeTe using angle-resolved photoemission spectroscopy (ARPES), transport property measurements and scanning tunneling spectroscopy (STS). We observe a hallmark of an HF behavior in ARPES spectra: a sharp quasiparticle peak (QP) near the Γ point and its strong temperature dependence. The observed QP is attributed to Kondo hybridization between Fe $3d_{xy}$ and Te $5p_z$. The Kondo hybridization scenario is further supported by STS results, showing the Fano line shape and narrow hybridization gap. In this picture, the recovery of metallic behavior in the low-temperature region is due to the emergence of the strong QP around the Γ point. We also conducted a Heisenberg model calculation, suggesting the Kondo interaction may be responsible for the emergence of BAFM in FeTe. These results provide a unified perspective that the Kondo interaction determines the exotic physical and magnetic properties in FeTe.

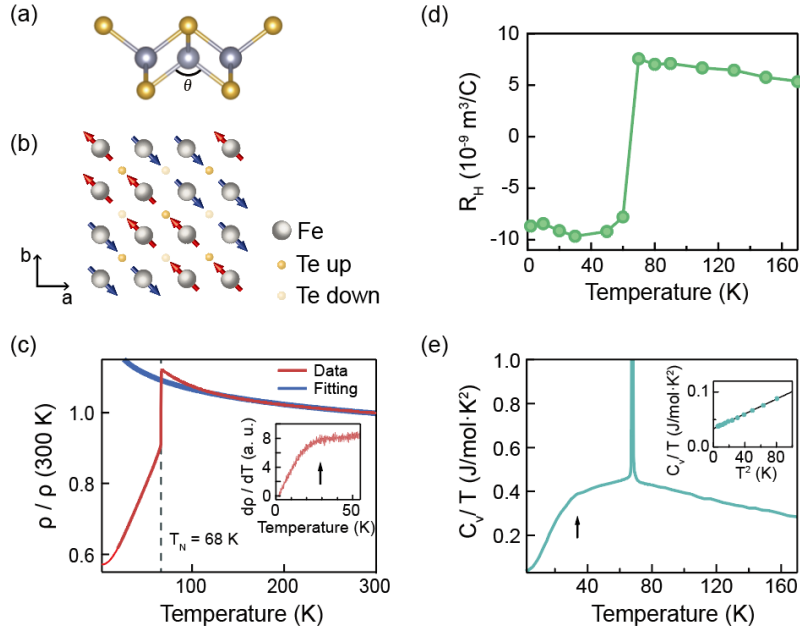


Fig. 1. Crystal structure and transport results of FeTe. (a) Crystal structure of FeTe. (b) Spin configuration of bicollinear antiferromagnetic (BAFM) state in FeTe. (c) Temperature-dependent resistivity. The red curve is the experimental data while the blue curve is the fitting result of the logarithmic function ($a + b \log(T)$) of the data between 120 K and 300 K. Inset shows the temperature-derivative of the resistivity. (d) Temperature-dependent Hall coefficient. (e) Temperature-dependent C_v/T . Inset shows C_v/T vs T^2 plot in the low-temperature region. The black solid line in the inset is the fit result of $C_v/T = \gamma + \beta T^2$.

II. RESULTS

A. TRANSPORT PROPERTIES

FeTe has the simplest crystal structure among the IBSCs as shown in Fig. 1(a). Compared to other similar iron chalcogenide systems of FeSe and FeS, FeTe has a distinctive bonding angle value θ shown in Fig 1(a). More specifically, Te atom is pushed away from the Fe plane due to its large atomic size and, as a result, FeTe has a small θ value [19]. This aspect of the crystal structure leads to localization of the Fe $3d_{xy}$ band as the d_{xy} orbital is confined in the Fe plane [13, 19]. A recent ARPES study showed a complete loss of coherent spectral weight in the d_{xy} band in FeTe, indicating a strong localization in the band [14, 20]. The magnetic ground state of FeTe is bicollinear antiferromagnetism (BAFM) as shown in Fig. 1(b) below a Néel temperature of near 70 K [18]. It is noteworthy that among IBSCs, only FeTe exhibits BAFM. The ordering vector of BAFM in FeTe is $(\pi/2, \pi/2)$ (1-Fe unit cell) while that of conventional AFM shown on other IBSCs is $(\pi, 0)$ [21].

Transport properties show a close relationship with magnetic properties. The temperature-dependent resistivity in Fig. 1(c) shows insulating behavior above T_N . We find the temperature dependence follows a logarithmic behavior of $-\ln(T)$. On the other hand, it abruptly recovers a metallic behavior below T_N . More specifically, it shows a Fermi liquid behavior below 30 K with a T^2 dependence resistivity, and a T -linear behavior between 30 K and 70 K. These T -

dependent behaviors indicate the existence of coherent-incoherent crossover around 30 K (see the inset of Fig. 1(c)). The Hall coefficient, as well as the resistivity, shows a drastic change at T_N . The Hall coefficient changes hole dominant ($T > T_N$) to electron dominant ($T < T_N$) at T_N as can be seen in Fig. 1(d). The crossover behavior seen in the resistivity data can be also found in the heat capacity data in Fig. 1(e); C_v/T deviates from T^2 behavior around 30 K. Further analysis shows that the Sommerfeld coefficient extracted from the heat capacity is $33.4 \text{ mJ/mol}\cdot\text{K}^2$ (see the inset of Fig. 1(e)). It is much larger than that of other iron chalcogenides. For instance, it is 3.8 and $6.9 \text{ mJ/mol}\cdot\text{K}^2$ for FeS and FeSe, respectively (16, 17).

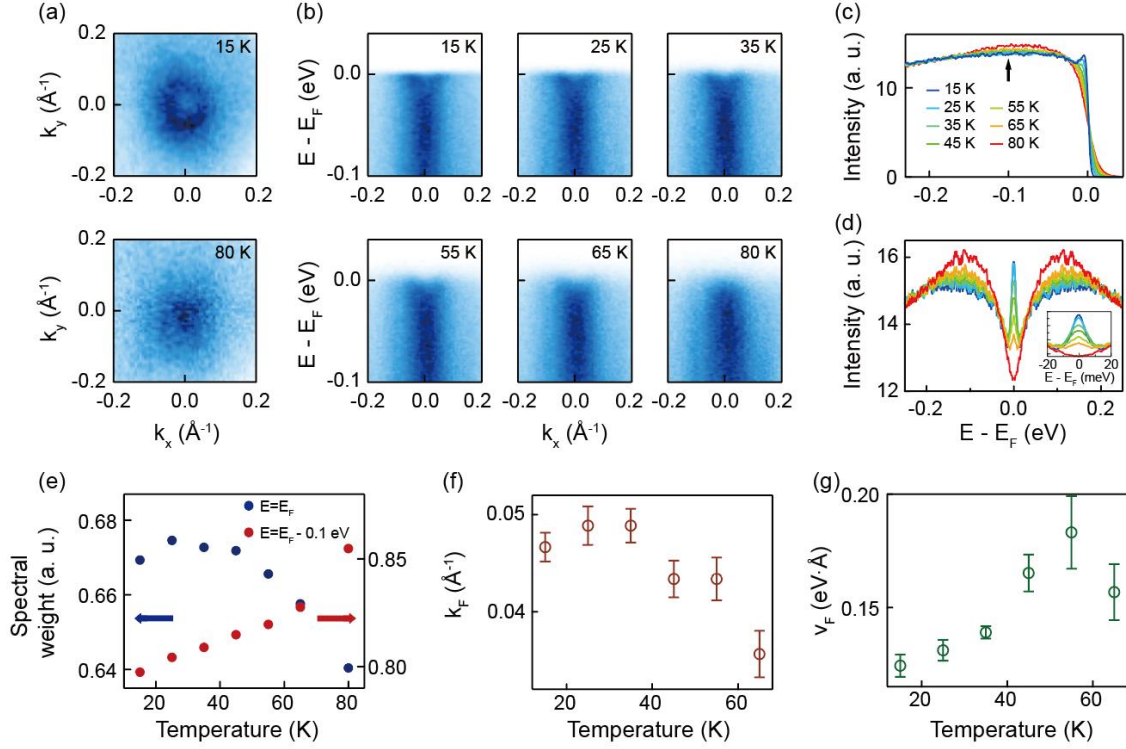


Fig. 2. Electronic structure of FeTe. (a) Fermi surface (FS) maps from high-resolution laser-ARPES measurements, obtained at 15 and 80 K. (b) Temperature-dependent high symmetry cuts along the Γ -X direction. ARPES data were taken with 11 eV photons. (c) Energy distribution curves (EDCs) integrated within a certain momentum range ($k_x^2 + k_y^2 < (0.15 \text{ \AA}^{-1})^2$). The EDCs are normalized with the integrated intensity from an energy window of $-0.25 \text{ eV} < E - E_F < -0.2 \text{ eV}$. (d) Symmetrized EDCs of (c). Inset: enlarged view of EDCs near the Fermi level. (e) Temperature-dependent spectral weight at $E = E_F$ and $E = E_F - 0.1 \text{ eV}$. (f and g) Temperature-dependent Fermi momentum (k_F) and Fermi velocity (v_F), respectively, obtained from momentum distribution curve (MDC) analysis. Errors bars in (f and g) represent the fitting errors of Fermi momentum and Fermi velocity, respectively.

B. ELECTRONIC STRUCTURES

We turn our attention to the electronic structure of FeTe. High-resolution laser ARPES experiments were performed to track the temperature-dependent evolution of the electronic structure. The Fermi surfaces (FSs) near the Γ point shown in Fig. 2(a) exhibit significant temperature dependence as the temperature decreases from 80 K to 15 K. A single circular FS

pocket is clearly observed at 15 K while it becomes a blob at 80 K. Evolution of the electronic structure can be also seen in the high symmetry cuts along the k_x -direction shown in Fig. 2(b). It is revealed that the FS pocket observed at 15 K in Fig. 2(a) comes from an electron band. As the temperature increases, the electron band tends to be broadened and vanishes abruptly at 80 K.

This observed temperature dependence of the band can be more clearly seen in the temperature-dependent energy distribution curves (EDCs) plotted in Fig. 2(c). A clear QP is observed at the lowest temperature, which comes from the electron band mentioned above. Upon increasing temperature, the QP is gradually suppressed while the spectral weight of the hump centered at -0.1 eV, indicated by an arrow in Fig. 2(c), gradually increases. Such spectral weight transfer behavior is more pronounced in symmetrized EDCs in Fig. 2(d). Analysis of the spectral weight transfer behavior is depicted in Fig. 2(e). It clearly shows that the lost QP spectral weight is transferred to the 0.1 eV hump, demonstrating that the observed temperature dependence is intrinsic. It is also noteworthy that the full width at half maximum (FWHM) of the QP obtained from a Lorentzian fitting is 7.9 meV as can be seen in the inset of Fig. 2(d), implying remarkable heavy mass and long quasiparticle lifetime of the band.

Additional band fitting analyses provide more information about the temperature-dependent evolution of the band. We extract the Fermi momentum (k_F) and Fermi velocity (v_F) using momentum distribution curve (MDC) analysis as depicted in Figs. 2(f) and 2(g), respectively. Temperature-dependent k_F value shows that the FS pocket size tends to enlarge upon cooling. Meanwhile, v_F of the electron band decreases with the temperature. From these results, we can infer that the temperature evolution of the k_F and v_F did not result from a simple chemical potential shift. The origin of the evolution will be discussed below.

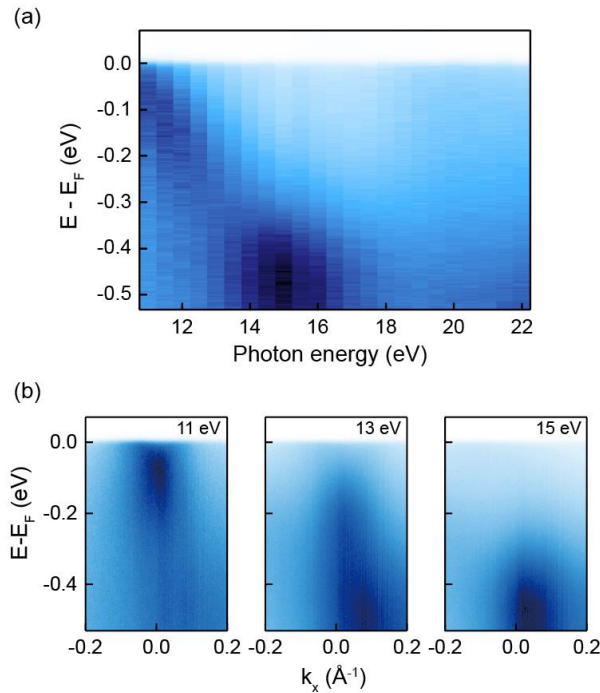


Fig. 3. Photon energy-dependent electronic structure. (a) Photon energy-dependent electronic structure near the Γ point. (b) Photon energy-dependent high symmetry cuts along the Γ -X direction, obtained using 11, 13, 15 eV photon.

The photon energy-dependent ARPES result gives further insights into the origin of the band. As can be seen in Fig. 3, the electron band which is clearly visible at 11 eV has a strong k_z dispersion. As the photon energy increases, the band shifts to the higher binding energy side, and its energy scale becomes more than 0.5 eV. Considering FeTe is in the strongly correlated limit, a bandwidth of 0.5 eV far surpasses that of Fe 3d bands [19]. In addition, the photoionization cross section of Te 5p orbital is much larger than that of Fe 3d orbital at 11 eV [22]. Thus, the band observed at 11 eV is likely to be mostly from Te p_z orbital. We note that similar k_z dispersion behavior was also reported for FeTe_{0.55}Se_{0.45} [23].

Considering the large dispersion of the p_z band away from E_F as shown in Fig. 3, the sharp QP near E_F implies that the band undergoes a strong modulation. Two scenarios may be considered for the modulation: (i) electron-bosonic mode coupling and (ii) Kondo hybridization between the itinerant and localized bands. It was claimed in a previous ARPES study on FeTe that the feature is a result of strong electron-phonon coupling, namely a polaronic behavior [24]. However, such a scenario may not explain the enlargement of the Fermi surface at low temperatures in Fig. 2(f) since an electron-boson coupling should conserve the k_F . Alternatively, one can consider a Kondo hybridization scenario which should also show a mass enhancement at low temperatures and strong temperature dependence of the QP. Therefore, it is highly desirable to have an alternative way to discern the two scenarios.

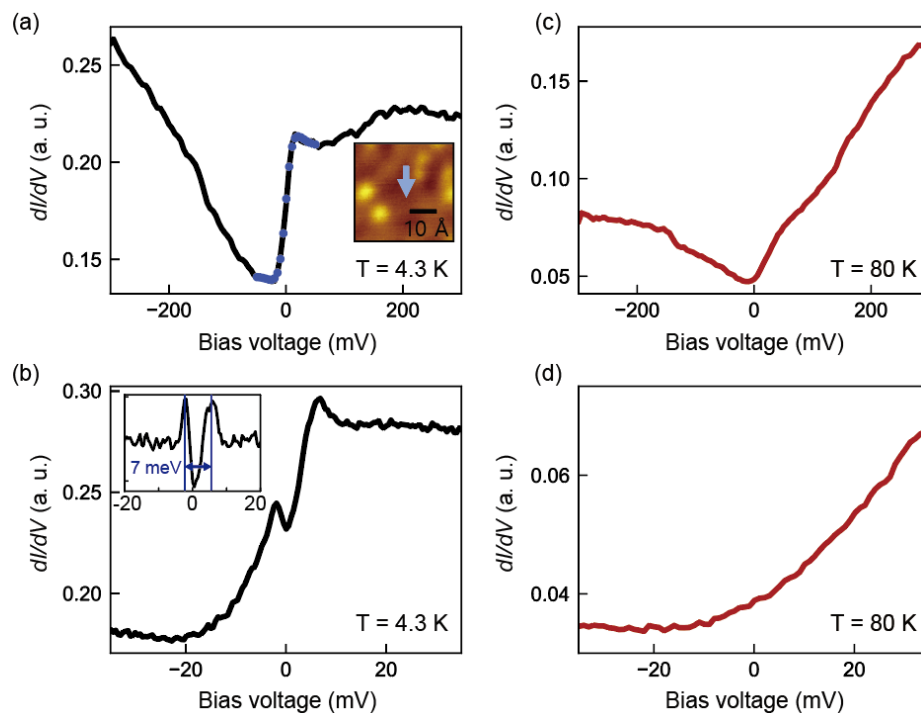


Fig. 4. STS results on FeTe. (a) Differential conductance (dI/dV) spectrum measured on FeTe surface at 4.3 K. The blue circles represent the Fano fitting of the Kondo resonance (see Supplemental Materials for the fitting parameters). The inset shows the position

where the spectrum is taken. $V_{\text{bias}} = -300$ mV, $I = 100$ pA and Lockin-modulation $V_{\text{mod}} = 5$ mV_{pp}. (b) dI/dV spectrum enlarged around the Fermi energy. The inset is the spectrum after subtracting the smoothly-varying background. $V_{\text{bias}} = -40$ mV, $I = 100$ pA and $V_{\text{mod}} = 500$ μ V_{pp}. (c) dI/dV spectra measured at 80 K. $V_{\text{bias}} = -300$ mV, $I = 50$ pA and $V_{\text{mod}} = 5$ mV_{pp}. (d) Zoomed-in dI/dV spectrum. $V_{\text{bias}} = -40$ mV, $I = 50$ pA and $V_{\text{mod}} = 500$ μ V_{pp}.

C. FANO LINE SHAPE AND HYBRIDIZATION GAP

Whether the strong renormalization of the dispersion near E_F is due to Kondo hybridization or not may be determined based on tunneling spectra. Shown in Fig. 4 are STS data at 4.3 and 80 K. A wide energy range scan at 4.3 K depicted in Fig. 4(a) shows an asymmetric spectrum. The spectrum is found to be well fitted with a Fano line shape as illustrated in the figure. It is well-known that tunneling spectra from a Kondo singlet state should exhibit a Fano-type resonance [13, 25]. Furthermore, a closer look of the data over a narrow energy range around E_F plotted in Fig. 4(b) shows a gap feature that is consistent with a gap expected for a Kondo hybridization scenario. We subtract the smoothly-varying background from the data and plot it in the inset. The subtracted data shows a gap with a size of about 7 meV as seen in Fig. 4(b). In addition, it is seen that the gap feature is slightly shifted to the unoccupied side. Plotted in Figs. 4(c) and 4(d) are dI/dV spectra taken at 80 K, above T_N . The two spectra are taken over the same energy ranges as the 4.3 K data. The Kondo-related features are expected to disappear at high temperatures, which are indeed seen in the high-temperature data in Figs. 4(c) and 4(d); the Fano behavior is weakened and the hybridization gap has disappeared. Therefore, these observations – Fano behavior and narrow gap near E_F – are clear signs of Kondo hybridization, confirming that FeTe exhibits Kondo hybridization below T_N .

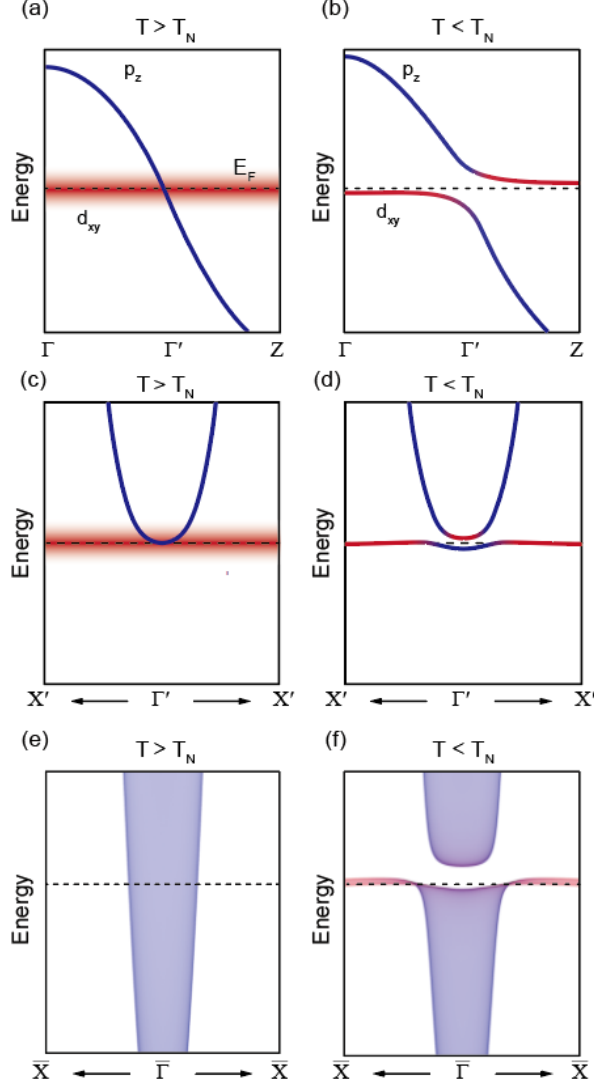


Fig. 5. Schematic of the Kondo hybridization scenario. (a and b) Band structure of FeTe along the Γ -Z direction (out-of-plane) above and below T_N , respectively. (c and d) Band structure of FeTe along the Γ -X direction (in-plane) above and below T_N , respectively. (e and f) Simulated band structure projected onto the (001) surface along the Γ -X direction (in-plane) above and below T_N , respectively. Blue bands denote p_z orbital, and red bands denote d_{xy} orbital.

III. DISCUSSIONS

A. KONDO HYBRIDIZATION SCENARIO

Fully considering our comprehensive data, we argue that the electron band that emerges below T_N is a result of a Kondo hybridization between the itinerant p_z and localized d_{xy} bands. When the system enters the BAFM state, the p_z and d_{xy} bands start to Kondo hybridize as illustrated in Fig. 5; the strongly dispersive p_z band along k_z direction crosses the localized d_{xy} band, resulting in a Kondo hybridization and heavy electron band. The correlation between Kondo hybridization and BAFM is discussed later. Based on known band dispersions, we simulate the

band structure with a finite hybridization between the p_z and d_{xy} band. The simulated band structures projected onto the (001) surface in Figs. 5(e) and (f) well coincide with ARPES results shown in Fig. 2(b) at the temperature of 80 K and 15 K, respectively. In addition, the narrow gap in the unoccupied side at low temperature and its disappearance at high temperature in the STS data directly support the band diagram illustrated in Fig. 5(f) and (e), respectively. The details of the simulation are described in the Materials and Methods section. The Kondo hybridization scenario is further supported by previous inelastic neutron scattering measurements on FeTe: the study reported that the local magnetic moment of FeTe is $S = 1$ at 10 K but it unexpectedly grows to $S = 3/2$ at 300 K, suggesting low-temperature Kondo screening of the local moments by itinerant electrons [26]. Note that the d_{xy} band is not visible near the Fermi level since d_{xy} band is strongly localized and thus its spectral weight near the Fermi level is mostly transferred to the high binding energy region and the photoionization cross section of Te 5p orbitals far surpass that of Fe 3d orbitals at 11 eV photon [20, 23].

The observed heavy electron band resulting from Kondo hybridization can address the unique transport properties of FeTe: (i) recovery of metallic behavior below T_N , (ii) sudden sign change in the Hall conductivity at T_N , and (iii) emergent Fermi liquid behavior at low temperature. First, the recovery of metallic behavior can be understood through the emergence of the sharp and strong QP at the Fermi level near the Γ point at T_N ; the transport properties are dominated by the QP. The emergence of the electron QP below T_N can also explain the sign change in the Hall conductivity, from hole dominant ($T > T_N$) to electron dominant ($T < T_N$). A previous study reported that recovery of the metallic behavior and Hall coefficient change may be related to the formation of pseudogap near the Brillouin zone corner [27]. However, their observation is not enough to explain the abrupt change in the resistivity and Hall conductivity. Thus, we believe the FS near the Γ point, which exhibits a sudden change at T_N , dominates transport properties. Finally, the sharp QP bandwidth of 7.9 meV indicates a long quasiparticle lifetime, indicating that FeTe is in a Fermi liquid regime at low temperatures. This observation is consistent with the unique transport results and enhanced Sommerfeld coefficient of FeTe.

The overall temperature dependence of electronic structures and transport properties are well explained within the Kondo lattice scenario. In the paramagnetic (PM) state, FeTe is in the Kondo scattering regime, consistent with the logarithmic resistivity [28, 29]. From the electronic structure point of view, the strong scattering induced in the Kondo scattering regime leads to a loss of coherence which results in a strong hump structure at high binding energy and weak spectral weight near the Fermi level [28, 30]. On the other hand, when the system enters the BAFM state, low-temperature behaviors of a Kondo lattice emerge: a sharp quasiparticle peak in the electronic structure induced by Kondo hybridization [28, 31] as well as a Fermi liquid behavior (T^2 dependence) at low temperature followed by a coherent-incoherent crossover in resistivity [8, 13, 26]. Based on these facts, we may address the unique feature of the Kondo lattice behavior in FeTe; low-temperature Kondo lattice behaviors in FeTe suddenly set in at the onset of BAFM as evidenced by the abrupt drop in the resistivity and sudden emergence of QP at T_N . This drastic shift of the system to the low-temperature Kondo lattice regime at the onset of the BAFM suggests a possible positive correlation between BAFM and Kondo lattice behavior in FeTe.

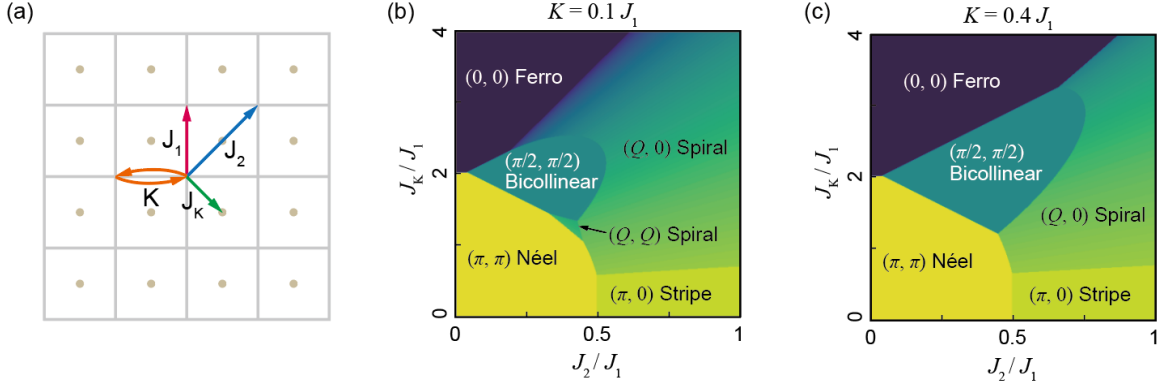


Fig. 6. Magnetic phase diagram of FeTe from Heisenberg model. (a) Definition of the Heisenberg model parameters. Grey solid lines denote the prime square lattice, whereas brown dots denote sublattice. J_1 and J_2 are nearest-neighbor (NN) and next nearest-neighbor (NNN) exchange interactions, respectively, on the prime lattice. J_K denotes NN exchange interaction between the prime lattice and sublattice. K is the NN biquadratic exchange interaction. (b, c) Magnetic phase diagram calculated from the model Hamiltonian (Eqn. 1) with $K = 0.1$ and 0.4 , respectively.

B. KONDO INTERACTION AND MAGNETISM

To reveal the underlying mechanism of the positive correlation between BAFM and Kondo lattice behavior in FeTe, we conducted a Heisenberg model calculation with an additional Fe-Te exchange interaction. Based on the established two-neighbor Heisenberg model with the biquadratic term (J_1 - J_2 - K model) on a prime square lattice [32-35], we additionally introduce a centered sublattice as shown in Fig. 5(a) to take into account the Fe-Te interaction (defined as J_K hereafter). We define the J_1 - J_2 - J_K - K model on the combined lattice as

$$H = J_1 \sum_{\langle i,j \rangle} \vec{S}_i \cdot \vec{S}_j - K \sum_{\langle i,j \rangle} (\vec{S}_i \cdot \vec{S}_j)^2 + J_2 \sum_{\langle\langle i,j \rangle\rangle} \vec{S}_i \cdot \vec{S}_j + J_K \sum_{\langle i,k \rangle} \vec{S}_i \cdot \vec{S}_k$$

where J_1 and J_2 are nearest-neighbor (NN) and next nearest-neighbor (NNN) exchange interactions on the prime lattice, respectively, and K is the NN biquadratic exchange interaction, while J_K is the NN interaction between prime lattice and sublattice as described in Fig. 6(a). i and j are indices for the prime lattice, and k is the sublattice index.

We solved the J_1 - J_2 - J_K - K model for various K values and obtained the corresponding magnetic phase diagram in Fig. 6(b) and (c). For a small J_K , the model well reproduces $(\pi, 0)$ stripe phase in iron pnictides. As J_K grows, $(\pi/2, \pi/2)$ BAFM starts to be stabilized and spans the phase diagram over a wide range of K (see Supplemental Materials for an extended phase diagram.). Within the J_K -induced BAFM scenario, the sublattice (Te atom for FeTe) should be also spin-polarized accordingly. We note that previous spin-polarized scanning tunneling microscopy measurements on FeTe revealed that Te atoms are also spin-polarized in the BAFM state [36]. These results suggest that J_K , an exchange interaction between Fe and Te, may play a crucial role in stabilizing the BAFM in FeTe. This J_K -induced BAFM scenario thus explains the positive correlation between Kondo lattice behavior and BAFM since the Kondo lattice behavior and BAFM share the same origin, J_K . The positive correlation between long-range

magnetism and Kondo lattice state is reminiscent of the underscreened Kondo lattice model in UTe and $\text{UCu}_{0.9}\text{Sb}_2$, where a local magnetic moment of $S = 1$ is not fully screened by itinerant electrons [37-38]. Likewise, the local moment of $S = 3/2$ in FeTe at 300 K is not fully screened, resulting in a residual local moment of $S = 1$ at 10 K [26], suggesting a possible analogy with the underscreened Kondo lattice model.

We find the J_1 - J_2 - J_K -K model has further implications. It was previously reported that an unexpected ferromagnetic (FM) state emerges under hydrostatic pressure [39]. A transition from BAFM to FM occurs in our calculated magnetic phase diagram if J_K is further increased. Note that previously proposed Heisenberg models had to employ the third nearest-neighbor exchange interaction (J_3) to account for the BAFM in FeTe, but could not predict the FM phase [34, 35]. In other words, the inclusion of J_K may be the key to understanding the magnetic order in FeTe.

IV. SUMMARY AND OUTLOOK

Recently, there have been numerous studies reporting that orbital-selectiveness is a prominent ingredient to make physics diverse in correlated d-electron multiorbital systems [14, 40-44]. In particular, while the orbital-selective Mott phase itself is an intriguing phenomenon, another important aspect is that materials with orbital-selective Mott phase are vulnerable to Kondo hybridization and thus may result in a new type of HF state [8-10]. We thus suppose that the local magnetic moment formed in the orbital-selective Mott phase critically affects the physical and magnetic properties of FeTe via Kondo interaction [14]. Our results shed light on the role of the local magnetic moments in correlated d-electron multiorbital systems.

APPENDIX. A: MATERIALS AND METHODS

Sample growth and characterization

Single crystals of FeTe were synthesized using a modified Bridgman method [45]. Stoichiometric iron (99.99 %) and tellurium (99.999 %) were sealed into an evacuated quartz tube and placed in a two-zone furnace. The hot (cold)-zone of the furnace was set to be 1070 (970) °C and slowly cooled down to 570 (470) °C at a rate of 2 °C/h. The stoichiometry was determined by energy dispersive X-ray spectrometry and found to be almost stoichiometric.

ARPES measurements

High-resolution ARPES measurements were performed with a home lab-based laser ARPES system equipped with a 10.897 eV laser (UV-2 from Lumeras) and a time-of-flight analyzer (ARTOF 10k from Scienta Omicron) [46]. Photon energy-dependent ARPES measurements were performed at BL-21B1 of the National Synchrotron Radiation Research Center (NSRRC). All ARPES measurements were conducted with p-polarized light. Overall energy resolution for the laser ARPES and photon energy dependent ARPES measurements was set to be 2 and 14 meV, respectively. The temperature dependent measurements were conducted upon cooling, starting from 80 K. The photon energy-dependent measurements were conducted at 15 K.

Transport measurements

The resistivity and heat capacity measurements were carried out with a Physical Property Measurement System (PPMS from Quantum Design). The resistivity and Hall coefficient measurement was conducted in a standard 4-probe and Hall bar geometry, respectively.

STM measurements

STM experiments have been performed using a home-built low-temperature STM operating at 4.3 K or 80 K. The FeTe single crystal precooled to 15 K was cleaved in the ultra-high vacuum condition. The cleaved FeTe sample was immediately inserted into the STM head. An PtIr tip is used for the measurements, and the tip quality is checked by the surface interference pattern on Cu(111). To acquire dI/dV spectra, a standard lock-in technique was used with a modulation frequency of $f = 718$ Hz.

Band structure simulation

The band structure simulation with a toy model is conducted to simulate ARPES results with finite k_z broadening where a strongly k_z -dispersive band is hybridized with a localized band. The simulation is based on a two-band model with a finite hybridization. The Hamiltonian is defined as

$$H = \begin{pmatrix} E_p(\vec{k}) & \Delta \\ \Delta & E_d(\vec{k}) \end{pmatrix},$$

where

$$E_p(\vec{k}) = 5t \left(\frac{k_x}{\pi} \right)^2 + 100t \cos(k_z) - \mu,$$
$$E_d(\vec{k}) = -\frac{t}{200} \left(\frac{k_x}{\pi} \right)^2 - t \cos(k_z) - \mu,$$

$$\Delta = 10t.$$

t is the energy scale of the hopping parameter and μ is the chemical potential of the system which is set arbitrarily. The basis of each axis is p, d orbitals, respectively. The in-plane dispersion is defined as parabolic and out-of-plane dispersion is defined as a cosine function. The dispersion parameter is based on the DFT calculation and ARPES results on $\text{FeTe}_{1-x}\text{Se}_x$ [20, 22-24]. The diagonalized band structures are projected onto the (001) surface and plotted in Fig. 5(f). For Fig. 5(e), only $E_p(\vec{k})$ is plotted to simulate the ARPES data at 80 K where hybridization does not occur. The blue and red intensity in Fig. 5 denotes the orbital character of p_z and d_{xy} , respectively.

ACKNOWLEDGEMENTS

The authors appreciate valuable discussion with Prof. T. Tohyama. This work was supported by the Institute for Basic Science in Korea (Grant No. IBS-R009-G2). The work at Yonsei University was supported by the National Research Foundation of Korea (NRF) [grant numbers NRF-2017R1A5A1014862 (SRC program: vdWMRC center), and NRF-2019R1A2C2002601].

REFERENCES

- [1] A. Ramirez, *Colossal magnetoresistance*, J. Condens. Matter Phys. **9**, 8171 (1997).
- [2] N. Nagaosa, J. Sinova, S. Onoda, A. H. MacDonald, N. P. Ong, *Anomalous hall effect*, Rev. Mod. Phys. **82**, 1539 (2010).
- [3] N. D. Mathur, F. M. Grosche, S. R. Julian, I. R. Walker, D. M. Freye, R. K. W. Haselwimmer and G. G. Lonzarich, *Magnetically mediated superconductivity in heavy fermion compounds*, Nature **394**, 39-43 (1998).
- [4] P. Monthoux, D. Pines, G. Lonzarich, *Superconductivity without phonons*, Nature **450**, 1177-1183 (2007).
- [5] P. Noël, F. Trier, L. M. V. Arche, J. Bréhin, D. C. Vaz, V. Garcia, S. Fusil, A. Barthélémy, L. Vila, M. Bibes and Jean-Philippe Attané., *Non-volatile electric control of spin-charge conversion in a SrTiO₃ Rashba system*, Nature **580**, 483-486 (2020).
- [6] S. G. Stewart, *Heavy-fermion systems*, Rev. Mod. Phys. **56**, 755 (1984).
- [7] S. Wirth, F. Steglich, *Exploring heavy fermions from macroscopic to microscopic length scales*, Nat. Rev. Mater. **1**, 1-16 (2016).
- [8] Y. P. Wu, D. Zhao, A. F. Wang, N. Z. Wang, Z. J. Xiang, X. G. Luo, T. Wu, and X. H. Chen, *Emergent Kondo Lattice Behavior in Iron-Based Superconductors AFe₂As₂ (A=K, Rb, Cs)*, Phys. Rev. Lett. **116**, 147001 (2016).
- [9] M. Kim, J. Kwon, C. H. Kim, Y. Kim, D. Chung, H. Ryu, J. Jung, B. S. Kim, D. Song, J. D. Denlinger, *et al.*, *Observation of Kondo hybridization with an orbital-selective Mott phase in 4d Ca_{2-x}Sr_xRuO₄*, arXiv:2102.09760 (2021).
- [10] D. Zhao, S. J. Li, N. Z. Wang, J. Li, D. W. Song, L. X. Zheng, L. P. Nie, X. G. Luo, T. Wu, and X. H. Chen, *Breakdown of single spin-fluid model in the heavily hole-doped superconductor CsFe₂As₂*, Phys. Rev. B **97**, 045118 (2018).
- [11] A. Shimoyamada, S. Tsuda, K. Ishizaka, T. Kiss, T. Shimojima, T. Togashi, S. Watanabe, C. Q. Zhang, C. T. Chen, Y. Matsushita, H. Ueda, Y. Ueda, and S. Shin, *Heavy-Fermion-like State in a Transition Metal Oxide LiV₂O₄ Single Crystal: Indication of Kondo Resonance in the Photoemission Spectrum*, Phys. Rev. Lett. **96**, 026403 (2006).
- [12] K.-J. Xu, S.-D. Chen, Y. He, J. He, S. Tang, C. Jia, E. Y. Ma, S.-K. Mo, D. Lu, M. Hashimoto, T. P. Devereaux, and Z.-X. Shen, *Metallic surface states in a correlated d-electron topological Kondo insulator candidate FeSb*, Proc. Natl. Acad. Sci. U.S.A. **27**, 117 (2020).
- [13] Y. Zhang, H. Lu, X. Zhu, S. Tan, W. Feng, Q. Liu, W. Zhang, Q. Chen, Y. Liu, X. Luo, D. Xie, L. Luo, Z. Zhang and X. Lai, *Emergence of Kondo lattice behavior in a van der Waals itinerant ferromagnet, Fe₃GeTe₂*, Sci. Adv. **4**, 1, eaao6791 (2018).
- [14] Z. P. Yin, K. Haule and G. Kotliar, *Kinetic frustration and the nature of the magnetic and paramagnetic states in iron pnictides and iron chalcogenides*, Nat. Mater. **10**, 932-935 (2011).
- [15] P. K. Maheshwari, V. R. Reddy and V. P. S. Awana, *Heat Capacity and Mössbauer Study of Self-Flux Grown FeTe Single Crystal*, J. Supercond. Nov. Magn. **31**, 1659–1663 (2018).

- [16] J. Xing, H. Lin, Y. Li, S. Li, X. Zhu, H. Yang, and H.-H. Wen, *Nodal superconducting gap in tetragonal FeS*, Phys. Rev. B **93**, 104520 (2016).
- [17] L. Wang, F. Hardy, T. Wolf, P. Adelman, R. Fromknecht, P. Schweiss, and C. Meingast, *Superconductivity-enhanced nematicity and “s+d” gap symmetry in Fe(Se_{1-x}S_x)*, Phys. Status Solidi B **254**, 1600153 (2017).
- [18] J. Jiang, C. He, Y. Zhang, M. Xu, Q. Q. Ge, Z. R. Ye, F. Chen, B. P. Xie, and D. L. Feng, *Distinct in-plane resistivity anisotropy in a detwinned FeTe single crystal: Evidence for a Hund's metal*, Phys. Rev. B **88**, 115130 (2013).
- [19] M. Yi, Y. Zhang, Z.-X. Shen and D. Lu, *Role of the orbital degree of freedom in iron-based superconductors*, npj Quantum Mater. **2**, 57 (2017).
- [20] J. Huang, R. Yu, Z. Xu, J.-X. Zhu, J. S. Oh, Q. Jiang, M. Wang, H. Wu, T. Chen, J. D. Denlinger, S.-K. Mo, M. Hashimoto, M. Michiardi, T. M. Pedersen, S. Gorovikov, S. Zhdanovich, A. Damascelli, G. Gu, P. Dai, J.-H. Chu, D. Lu, Q. Si, R. J. Birgeneau and M. Yi, *Correlation-driven electronic reconstruction in FeTe_{1-x}Se_x*, Commun. Phys. **5**, 29 (2022).
- [21] T. J. Liu, J. Hu, B. Qian, D. Fobes, Z. Q. Mao, W. Bao, M. Reehuis, S. A. J. Kimber, K. Proke, S. Matas, D. N. Argyriou, A. Hiess, A. Rotaru, H. Pham, L. Spinu, Y. Qiu, V. Thampy, A.T. Savici, J. A. Rodriguez, and C. Broholm, *From (π , 0) Magnetic Order to Superconductivity with (π , π) Magnetic Resonance in Fe_{1.02}Te_{1-x}Se_x*, Nat. Mater. **9**, 718 (2010).
- [22] X.-L. Peng, Y. Li, X.-X. Wu, H.-B. Deng, X. Shi, W.-H. Fan, M. Li, Y.-B. Huang, T. Qian, P. Richard, J.-P. Hu, S.-H. Pan, H.-Q. Mao, Y.-J. Sun, and H. Ding, *Observation of topological transition in high-T_C superconducting monolayer FeTe_{1-x}Se_x films on SrTiO₃(001)*, Phys. Rev. B **100**, 155134 (2019).
- [23] Z. Wang, P. Zhang, G. Xu, L. K. Zeng, H. Miao, X. Xu, T. Qian, H. Weng, P. Richard, A. V. Fedorov, H. Ding, X. Dai, and Z. Fang, *Topological nature of the FeSe_{0.5}Te_{0.5} superconductor*, Phys. Rev. B **92**, 115119 (2015).
- [24] Z. K. Liu, R.-H. He, D. H. Lu, M. Yi, Y. L. Chen, M. Hashimoto, R. G. Moore, S.-K. Mo, E. A. Nowadnick, J. Hu, *et al.*, *Measurement of Coherent Polarons in the Strongly Coupled Antiferromagnetically Ordered Iron-Chalcogenide Fe_{1.02}Te using Angle-Resolved Photoemission Spectroscopy*, Phys. Rev. Lett. **110**, 037003 (2013).
- [25] P. Aynajian, E. H. da Silva Neto, C. V. Parker, Y. Huang, A. Pasupathy, J. Mydosh, and A. Yazdani, *Visualizing the formation of the Kondo lattice and the hidden order in URu₂Si₂*, Proc. Natl. Acad. Sci. U.S.A. **107**, 10383–10388 (2010).
- [26] I. A. Zaliznyak, Z. Xu, J. M. Tranquada, G. Gu, A. M. Tsvelik, and M. B. Stone, *Unconventional Temperature Enhanced Magnetism in Fe_{1.1}Te*, Phys. Rev. Lett. **107**, 216403 (2011).
- [27] P. H. Lin *et al.*, *Nature of the bad metallic behavior of Fe_{1.06}Te inferred from its evolution in the magnetic state*, Phys. Rev. Lett. **111**, 217002 (2013).
- [28] S. Jang *et al.*, *Evolution of the Kondo lattice electronic structure above the transport coherence temperature*, Proc. Natl. Acad. Sci. U.S.A. **117**, 38 23467-23476 (2020).
- [29] J. Kondo, *Resistance Minimum in Dilute Magnetic Alloys*, Prog. Theor. Phys. **32**, 1, 37-49 (1964).

- [30] M. J. Rozenberg, G. Kotliar, H. Kajueter, *Transfer of spectral weight in spectroscopies of correlated electron systems*, Phys. Rev. B. **54**, 12, 8452 (1996).
- [31] S. Patil *et al.*, *ARPES view on surface and bulk hybridization phenomena in the antiferromagnetic Kondo lattice CeRh₂Si₂*, Nat. Commun. **7**, 11029 (2016).
- [32] A. N. Yaresko, G.-Q. Liu, V. N. Antonov, O. K. Andersen, *Interplay between magnetic properties and Fermi surface nesting in iron pnictides*, Phys. Rev. B **79**, 144421 (2009).
- [33] A. L. Wysocki, K. D. Belashchenko, V. P. Antropov, *Consistent model of magnetism in ferropnictides*, Nat. Phys. **7**, 485–489 (2011).
- [34] J. Hu, B. Xu, W. Liu, N.-N. Hao and Y. Wang, *Unified minimum effective model of magnetic properties of iron-based superconductors*, Phys. Rev. B **85**, 144403 (2012).
- [35] J. K. Glasbrenner, I. I. Mazin, Harald O. Jeschke, P. J. Hirschfeld, R. M. Fernandes and Roser Valentí, *Effect of magnetic frustration on nematicity and superconductivity in iron chalcogenides*, Nat. Phys. **11**, 953-958 (2015).
- [36] M. Enayat, Z. Sun, U. R. Singh, R. Aluru, S. Schmaus, A. Yaresko, Y. Liu, C. Lin, V. Tsurkan, A. Loidl *et al.*, *Real-space imaging of the atomic-scale magnetic structure of Fe_{1+y}Te*, Science **345**, 6197, 653-656 (2014).
- [37] N. B. Perkins, M. D. Núñez-Regueiro, B. Coqblin, and J. R. Iglesias, *Underscreened Kondo lattice model applied to heavy fermion uranium compounds*, Phys. Rev. B **76**, 125101 (2007)
- [38] B. Coqblin, J. R. Iglesias, N. B. Perkins, S. G. Magalhães, F. M. Zimmer, *Doniach diagram for ordered, disordered and underscreened Kondo lattices*, J. Magn. Mater. **320**, 1989-1994 (2008).
- [39] M. Bendele, A. Maisuradze, B. Roessli, S. N. Gvasaliya, E. Pomjakushina, S. Weyeneth, K. Conder, H. Keller, and R. Khasanov, *Pressure-induced ferromagnetism in antiferromagnetic Fe_{1.03}Te*, Phys. Rev. B **87**, 060409(R) (2013).
- [40] P. O. Sprau *et al.*, *Discovery of orbital-selective Cooper pairing in FeSe*, Science **357**, 75-80 (2017).
- [41] M. Yi *et al.*, *Observation of universal strong orbital-dependent correlation effects in iron chalcogenides*, Nat. Commun. **6**, 7777 (2015).
- [42] L. de' Medici, *Hund's coupling and its key role in tuning multiorbital correlations*, Phys. Rev. B **83**, 205112 (2011).
- [43] M. Yi *et al.*, *Observation of temperature-induced crossover to an orbital-selective Mott phase in A_xFe_{2-y}Se₂ (A= K, Rb) superconductors*, Phys. Rev. Lett. **110**, 067003 (2013).
- [44] G. Lee *et al.*, *Orbital selective Fermi surface shifts and mechanism of high T_C superconductivity in correlated AFeAs (A=Li, Na)*, Phys. Rev. Lett. **109**, 177001 (2012).
- [45] G. F. Chen *et al.*, *Electronic properties of single-crystalline Fe_{1.05}Te and Fe_{1.03}Se_{0.30}Te_{0.70}*, Phys. Rev. B **79**, 140509 (2009).
- [46] Y. He *et al.*, *Invited article: High resolution angle resolved photoemission with tabletop 11 eV laser*, Rev. Sci. Instrum. **87**, 011301 (2016).